






Performance of Joint Sensing-Communication Cooperative Sensing UAV Network

Xu Chen , Student Member, IEEE, Zhiyong Feng , Senior Member, IEEE, Zhiqing Wei , Member, IEEE, Feifei Gao , Fellow, IEEE, and Xin Yuan , Member, IEEE

Abstract—To exploit the spectrum reuse potential and enhance the cooperative sensing ability of the cooperative sensing unmanned aerial vehicle network (CSUN), we propose a novel joint sensing-communication (JSC) CSUN that can simultaneously conduct downward-looking radar sensing and sensing data fusion communication with the unified spectrum and transceiver by adopting the beam sharing scheme. To achieve the beam sharing scheme, we design a novel antenna array equipped on each UAV, which can generate a sensing beam and a communication beam orthogonally for downward detection and data-fusion communication, respectively. To quantify the cooperative sensing performance of CSUN, we propose and formulate a novel upper-bound average cooperative sensing area (UB-ACSA) as the cooperative sensing performance metric, based on deriving the closed-form expressions for the average mutual sensing interference of CSUN and the communication capacity constraints. Finally, extensive simulations are conducted to validate the theoretical results. We also demonstrate that the cooperative sensing performance of the JSC CSUN can improve by 66.3 percent compared with the conventional CSUN in terms of UB-ACSA.

Index Terms—Beam sharing, cooperative sensing, joint sensing-communication system, unmanned aerial vehicle network.

I. INTRODUCTION

A. Background and Motivations

BY NETWORKING multiple UAVs through radio communication, the UAV network can be formed to integrate the sensing data from multiple UAVs, and the sensing zone of the UAV network can be extended far beyond the limit of an

individual UAV [2], which is the aim of the cooperative sensing UAV network (CSUN). CSUN can finish detecting a large area in a much shorter time and gather more environmental information than an individual UAV, which enables CSUN to make decisions from a big picture perspective [2].

The conventional CSUN uses individually designed radar sensing and communication modules, occupying separate spectrum and transceivers. Thus, due to load and spectrum restrictions, the conventional CSUN is limited in improving the cooperative sensing performance. In this case, the joint sensing-communication (JSC) technique can be used as a reasonable solution to compensate the above constraints by providing load-saving and spectrum-reusing through using the unified transceivers and spectrum [2], [3]. As the digital multi-input multi-output (MIMO) millimeter-wave (mmWave) radar and communication devices have become similar in digital signal processing and transceiver design [4], [5], the concept of the JSC CSUN has become feasible. Equipped with JSC devices, the JSC CSUN can significantly improve the communication capacity for cooperative sensing [4] and the cooperative sensing ability.

B. Related Works

The strong need and potential of the joint design of communication and sensing have motivated a number of important studies in the JSC technique. Sturm *et al.* [6] proposed a novel orthogonal frequency division multiplexing (OFDM) symbol-based JSC signal processing method, which overcomes the typical drawbacks of correlation-based radar signal processing and satisfies both the radar ranging and communication requirements. In [7], the authors proposed a unified and reconfigurable multifunctional receiver for data-fusion services of radar sensing and radio communication based on time-division platform. In each time slot assigned for radar and radio communication modes, the system can offer positioning function and data communication, respectively. However, the time-division scheme system cannot simultaneously and constantly operate radar and communication [7]. In [8], a new JSC system was proposed for mobile communication system based on multibeam-forming technique and time-division-duplex (TDD) framework. In [9], Liu *et al.* proposed novel beamforming techniques that take signal-to-interference-and-noise ratio (SINR) constraints into consideration for a MIMO JSC system, which enables a base station to simultaneously communicate with downlink users and

Manuscript received June 11, 2020; revised August 10, 2020; accepted November 26, 2020. Date of publication December 4, 2020; date of current version January 22, 2021. This work was supported in part by the National Natural Science Foundation of China under Grants 61631003, 61790553, 61941102, and in part by the Beijing Natural Science Foundation under Grant L192031. This work is based on a previous conference paper accepted by IEEE International Conference on Signal, Information and Data Processing (ICSIDP) 2019 [1]. The review of this article was coordinated by Dr. F. Tang. (Corresponding authors: Zhiyong Feng; Zhiqing Wei.)

Xu Chen, Zhiyong Feng, and Zhiqing Wei are with the Beijing University of Posts and Telecommunications, Key Laboratory of Universal Wireless Communications, Ministry of Education, Beijing 100 876, China (e-mail: chenxu96330@bupt.edu.cn; fengzy@bupt.edu.cn; weizhiqing@bupt.edu.cn).

Feifei Gao is with the Institute for Artificial Intelligence, Tsinghua University (THUI), State Key Lab of Intelligent Technologies and Systems, Tsinghua University, Beijing National Research Center for Information Science and Technology (BNRist), Department of Automation, Tsinghua University Beijing, Beijing 100084, China (e-mail: feifeigao@ieee.org).

Xin Yuan is with the Commonwealth Scientific and Industrial Research Organization (CSIRO), Sydney, New South Wales 2122, Australia (e-mail: xinyuan.bupt@gmail.com).

Digital Object Identifier 10.1109/TVT.2020.3042466

TABLE I
KEY PARAMETERS AND ABBREVIATIONS

Symbol	Description
FCUAV	The UAV acting as fusion center
SU	Secondary UAV
MCA	Maximum cooperating area
MCR	Maximum cooperating range, x_Q
SZ	Sensing zone
ACSA	Average cooperative sensing area
UB-ACSA	The upper bound of ACSA, $S_{CSA}(M)$
ComA	Communication subarray of JSC array
SenA	Sensing subarray of JSC array
ComB	Communication beam
SenB	Sensing beam
SPR	Sensing power ratio, β_R
TxA	The transmitting antenna array of SenA
RxA	The receiving antenna array of SenA
S-C pair	The pair of FCUAV and an SU that is transmitting sensing data
STP	Successful transmission probability
R_g	The inner radius of MCA
R_{max}	Maximum effective sensing range
G_p	OFDM symbol-based radar processing gain
R_i	The distance between SU_i and FCUAV
h	The flying altitude of UAVs

detect radar targets. Liu *et al.* also proposed a novel mmWave massive multi-input multi-output (mMIMO) TDD JSC system that considers the channel interference [4]. Although the TDD multibeam JSC system can operate communication and sensing simultaneously, it still can not ensure the continuous JSC operation for JSC users.

There also appear some significant studies on the CSUN. In [10], the authors proposed a cooperative UAV network that can achieve cooperative navigation by sharing sensing data of environment among UAVs. The authors in [11] proposed a CSUN to sense large infrastructure, which can shorten the time for detecting the entire area. In [5], CSUN that utilizes individually designed radar and communication devices, i.e., exploit separate spectrum and transceivers for radar and communication, was studied. However, these works on CSUN are only concerned with individually designed sensing and communication systems and without considering the JSC technique, which cannot exploit the spectrum reuse potential of radar and communication modules and is referred to as the conventional CSUN in this paper.

C. Our Contributions

In this paper, we consider a JSC CSUN that consists of a leader fusion center UAV and multiple secondary UAVs, where the fusion center UAV merges all the detection data from the secondary UAVs. We propose a novel JSC antenna composed of a sensing subarray and a communication subarray to achieve the beam sharing scheme to implement JSC technique. Moreover, we propose a novel upper-bound average cooperative sensing area (UB-ACSA) as the cooperative sensing performance metric of CSUN, based on deriving the closed-form maximum sensing range of UAVs. The main contributions of this paper are summarized as follows.

1) We design a novel JSC antenna array and present a corresponding iterative beamforming algorithm that can flexibly form SenB and ComB orthogonally, so that JSC CSUN can operate sensing and data-fusion communication simultaneously and continuously with the unified spectrum and transceiver.

2) We derive the closed-form expressions for mutual sensing interference (MSI) and maximum sensing range of UAVs, which is useful to determine the effective sensing range for each UAV in the CSUN.

3) We propose and formulate a closed-form UB-ACSA as the novel cooperative sensing performance metric for CSUN. Through simulation, we validate the theoretical result of UB-ACSA. Moreover, we present that our proposed JSC CSUN can improve UB-ACSA by 66.3 percent compared with the conventional CSUN.

D. Outline of This Paper

The remaining parts of this paper are organized as follows. Section II describes the system model. Section III provides the closed-form expression for UB-ACSA. In section IV, the numerical simulation of the previous theoretical results is presented. Section V concludes this paper.

Notations: Bold uppercase letters denote matrices (i.e., \mathbf{M}); bold lowercase letters denote column vectors (i.e., \mathbf{v}); scalars are denoted by normal font (i.e., γ); the entries of vectors or matrices are referred to with parenthesis, for instance, the q th entry of vector \mathbf{v} is $\mathbf{v}(q)$, and the entry of the matrix \mathbf{M} at the m th row and q th column is $\mathbf{M}(m, q)$; \mathbf{I}_Q is the identity matrix with dimension $Q \times Q$. Also, matrix superscripts $(\cdot)^H$, $(\cdot)^*$ and $(\cdot)^T$ denote Hermitian transpose, complex conjugate and transpose, respectively. Besides, we use $(\cdot)^{-1}$ to denote inverse of matrix, $(\cdot)^\dagger$ to denote the pseudo-inverse of the matrix, $\text{diag}(\mathbf{v})$ to denote a diagonal matrix with the entries of \mathbf{v} on the diagonal, $E(\cdot)$ to denote the expectation of random variable, and $\lfloor \cdot \rfloor$ to denote the floor function.

II. SYSTEM MODEL

A. Model of Cooperative JSC CSUN

We consider a JSC CSUN that consists of a fusion center UAV (FCUAV) and M secondary UAVs (SUs), where FCUAV integrates the sensing data from all the SUs, as illustrated in Fig. 1. The altitude of FCUAV is denoted as h , and the altitude of the i th SU is denoted as h_i . Each UAV is assumed to be equipped with a JSC antenna array to generate a sensing beam (SenB) and a communication beam (ComB) orthogonally for sensing and data-fusion communication, respectively. SenB is pointed downward and used to detect the targets on the ground. ComB points to FCUAV and transmits sensing data. FCUAV integrates all the sensing data from SUs through ComB and conducts downward detection through SenB. SUs detect the targets through SenB while simultaneously and continuously transmitting the sensing data to FCUAV through ComB. The design of the JSC antenna array and the corresponding beamforming methods are presented in the next subsection.

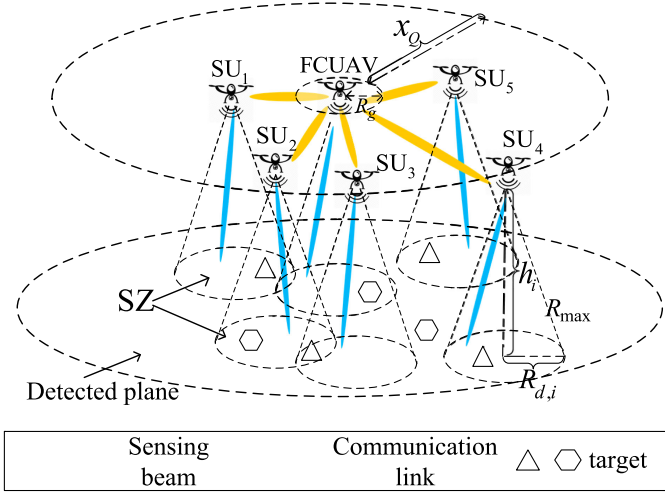


Fig. 1. The JSC UAV cooperative sensing network consists of a FCUAV and M SUs. The hovering of FCUAV is h , and the altitude of the i th SU is h_i . FCUAV integrates all the sensing data from SUs through ComB.

The antenna array of each UAV has available radio power P , i.e., the sum of SenB power and ComB power is P . The SenB power is given by

$$P_r = \beta_R P, \quad (1)$$

where β_R is defined as the sensing power ratio (SPR). The ComB power is thus $P_c = (1 - \beta_R)P$. OFDM waveform is adopted as the communication and sensing waveform to achieve joint communication and sensing [2]. Time division multiple access (TDMA) is adopted by the JSC CSUN to exploit the same frequency band to transmit sensing data. To ensure that FCUAV integrates the intact sensing data of each SU, the communication capacity between each SU and FCUAV has to be larger than the generating rate of sensing data. Therefore, the distance between FCUAV and each SU must be smaller than MCR, denoted by x_Q . Each UAV also has a guard radius R_g for safety, within which no other UAVs can hover. The area where SUs can hover is defined as the maximum cooperation area (MCA) whose inner and outer radii are R_g and x_Q , respectively.

Each UAV has to decrease the sensing signal power loss and reduce interference from other UAVs to maintain the minimum sensing SINR for satisfying the constraints on the false alarm rate and the detection probability [12], [13]. Thus, there is the maximum sensing range for each UAV, which is denoted by R_{\max} .

As shown in Fig. 1, the region on the ground that the JSC CSUN has to detect is defined as the detected plane. The region in the detected plane that can be effectively detected¹ by a UAV is defined as the sensing zone (SZ) of the UAV. The maximum radius of SZ is determined by R_{\max} and flying altitude. The average union area of SZs of all UAVs is proposed to be the sensing performance metric of the cooperative sensing CSUN, while the communication performance metric of the network

¹i.e., the false alarm rate is below the maximum and detection probability is higher than the minimum.

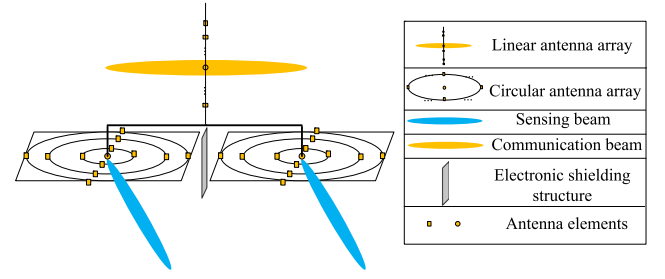


Fig. 2. The JSC antenna array is composed of a ComA and a SenA. The ComA is a ULA, and the SenA consists of two concentric circular arrays working as Tx and Rx, respectively. All antenna elements are isotropic.

is defined as the outage capacity of the links between SUs and FCUAV.

B. Beam Sharing Scheme and the Design of JSC Antenna Array

The beam sharing scheme is used to realize communication and sensing simultaneously. Let (φ, θ) be a certain direction in the three-dimensional (3D) space, where θ denotes the elevation angle and φ denotes the azimuth angle. ComA of each UAV generates ComB with elevation beamwidth² $\Delta\theta_c$ and azimuth beamwidth $\Delta\phi_c$. SenA of each UAV generates SenB with elevation beamwidth $\Delta\theta_r$ and azimuth beamwidth $\Delta\phi_r$.

The antenna array designed to achieve beam sharing consists of two parts, as illustrated in Fig. 2. The upper uniform linear array (ULA) is ComA that has M_{com} antenna elements with inter-distance half-wavelength. The lower subarray is SenA composed of two decoupled circular subarrays, where one is transmitting array (TxA) and the other is receiving array (RxA). TxA and RxA are used to generate transmitting SenB and receiving SenB, respectively. The electronic shielding plate is placed between two subarrays of SenA and the pulse response between two subarrays is also accurately measured to eliminate self-interference between TxA and RxA of SenA in real-time manner [14].

Two subarrays of SenA are used to solve the problem of minimum detection range by enabling receiver to work continuously [13]. If SenA adopts only one subarray, then it has to arrange time slots for transmitting and receiving the radar signal. In this case, the radar echo can return to SenA before the slot for receiving, and then the target may be lost. Only when the distance between UAV and the target is larger than the minimum value can the target be possibly detected, which is inapplicable to the situation where the target is close to the JSC units. By contrast, double subarrays of SenA enable the sensing signal to be transmitted and received continuously. Thus, the minimum detection range problem can be solved.

As illustrated in Fig. 3, SenA has antennas arranged in concentric circles. There are N_A circles in each SenA, and we define each circle as a layer. From center to periphery, SenA has the 0th layer to the $(N_A - 1)$ th layer. Except for the 0th layer with

²In this article, the term “beamwidth” refers to the -3 dB half-power beamwidth.

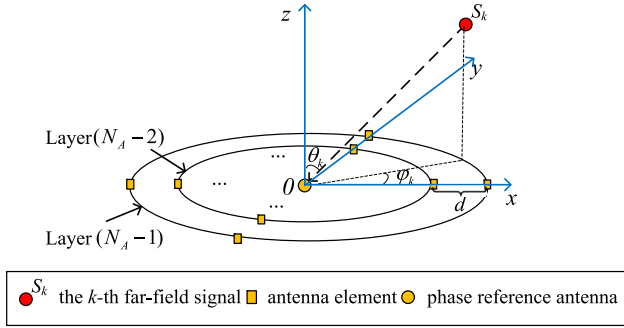


Fig. 3. The design of concentric circular SenA. There are N_A layers with each layer composed of 2^b antenna elements.

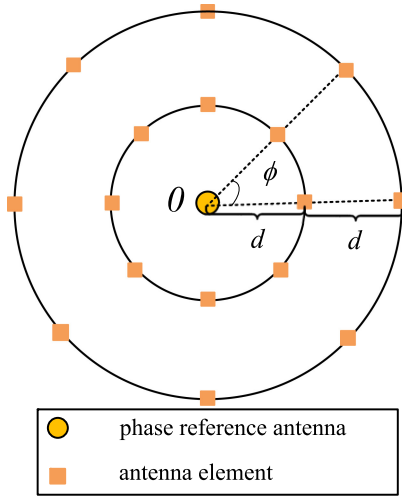


Fig. 4. Design of adjacent layers of SenA.

only one antenna element that is the phase reference antenna (PhRefA), there are 2^b antenna elements in each layer, where b is a positive integer. Fig. 4 shows the adjacent layers of SenA. The distance between the antennas that locate at the same polar angle of adjacent layers is d . Antennas in each layer locate at the evenly split angles, and are referred to as the 0th to the $(2^b - 1)$ th antenna, anti-clockwise.

C. Beamforming of JSC Antenna Array

1) *Beamforming of SenA*: Assume that there are K_s planar far-field signals arriving at SenA from different directions. The angle of arrival (AoA) of the k th ($k = 1, 2, \dots, K_s$) signal is $\mathbf{p}_k = (\varphi_k, \theta_k)^T$. We use $\Theta = \{\mathbf{p}_1, \dots, \mathbf{p}_{K_s}\}$ to denote the set of AoAs of all K_s signals.

Let $A_{p,q}$ be the q th antenna in the p th layer of SenA. The polar angle of $A_{p,q}$ is $\psi_{p,q} = q \cdot \phi$, where $\phi = \frac{2\pi}{2^b}$. For the k th signal with AoA \mathbf{p}_k , the phase difference between $A_{p,q}$ and PhRefA is given by

$$a_{p,q}(\mathbf{p}_k) = \exp \left\{ -j \frac{2\pi}{\lambda} \mathbf{P}_{p,q}^T \mathbf{v}_k \right\}, \quad (2)$$

where λ is the wavelength, and

$$\mathbf{v}_k = [\cos \varphi_k \sin \theta_k, \sin \varphi_k \sin \theta_k]^T, \\ \mathbf{P}_{p,q} = [p \cdot d \cos(\psi_{p,q}), p \cdot d \sin(\psi_{p,q})]^T.$$

Algorithm 1: Two-Step Iterative LS Beamforming Algorithm.

Input: The desired AoAs $\{\mathbf{p}_1, \mathbf{p}_2, \dots, \mathbf{p}_L\}$, and the corresponding steering matrix \mathbf{A} .
The desired amplitude pattern \mathbf{r}_{ad} .
Initial beamforming vector $\mathbf{w}_{r,0}$.
Iteration index $m = 0$.
Iteration time threshold τ_{th} .
Output: Final converged beamforming vector $\mathbf{w}_{r,m}$.
while $\mathbf{w}_{r,m}$ does not converge and $m \leq \tau_{th}$ **do**
1) $m = m + 1$.
2) $\mathbf{r}_{pd} = [\text{diag}(\mathbf{r}_{ad})]^{-1} \mathbf{A}^T \mathbf{w}_{r,m-1}^*$.
3) $\mathbf{r}_{pd1} = \frac{\mathbf{r}_{pd}}{|\mathbf{r}_{pd}|}$.
4) $\mathbf{w}_{r,m} = (\mathbf{A}^H)^{\dagger} [\text{diag}(\mathbf{r}_{ad})]^H \mathbf{r}_{pd1}^*$.
end
return $\mathbf{w}_{r,m}$

Furthermore, the steering vector of SenA is

$$\mathbf{a}(\mathbf{p}_k) = [1, a_{1,0}(\mathbf{p}_k), \dots, a_{N_A-1,2^b-1}(\mathbf{p}_k)]^T, \quad (3)$$

enumerating the phase differences between the PhRefA and all the other antenna elements of SenA. Then the steering matrix for K_s far-field signals is $\mathbf{A} = [\mathbf{a}(\mathbf{p}_1), \dots, \mathbf{a}(\mathbf{p}_{K_s})]$.

The received signal vector for SenA is

$$\mathbf{y} = \mathbf{A} \mathbf{s}_r + \mathbf{n}_s, \quad (4)$$

where \mathbf{s}_r is the source signal vector of dimension $K_s \times 1$, and \mathbf{n}_s is the additive white Gaussian noise (AWGN) with covariance matrix $\sigma_r^2 \mathbf{I}_{K_s}$ and zero mean.

Based on the least square (LS) error principle, the beamforming problem of SenA can be formulated as [15]

$$\min_{\mathbf{w}_r} \|\mathbf{w}_r^H \mathbf{A} - \mathbf{r}_d^T\|_2^2, \quad (5)$$

where \mathbf{w}_r is the normalized beamforming vector for SenA to generate SenB, and \mathbf{r}_d is the desired response, i.e.,

$$\mathbf{r}_d = \text{diag}(\mathbf{r}_{ad}) \times \mathbf{r}_{pd}, \quad (6)$$

where

$$\mathbf{r}_{ad} = [r_{ad}(\mathbf{p}_1), \dots, r_{ad}(\mathbf{p}_k)]^T,$$

$$\mathbf{r}_{pd} = [r_{pd}(\mathbf{p}_1), \dots, r_{pd}(\mathbf{p}_k)]^T,$$

representing the desired amplitude response and desired phase response, respectively. Note that \mathbf{r}_{ad} is a column vector of real values, and \mathbf{r}_{pd} is a column vector of complex values with unit modulus.

Two-step iterative LS beamforming method is presented to generate high-performance beam given AoAs [15], as shown in Algorithm 1. First, we determine the desired AoAs, amplitude response \mathbf{r}_{ad} and the corresponding steering matrix \mathbf{A} . Then we set the initial beamforming vector as $\mathbf{w}_{r,0} = \mathbf{0}$ and set the iteration time threshold as τ_{th} . If the iteration time m is smaller than τ_{th} , then the phase response \mathbf{r}_{pd} and the beamforming vector $\mathbf{w}_{r,m}$ are updated iteratively. After the iteration time reaches τ_{th} or $\mathbf{w}_{r,m}$ converges to a stable value, $\mathbf{w}_{r,m}$ is the output as the beamforming vector for SenB beamforming. In Algorithm 1, $|\mathbf{x}|$ brings out the vector where the i th entry is the

modulus of the i th entry of \mathbf{x} (\mathbf{x} can degrade to scalar), and $\frac{\mathbf{r}_{pd}}{|\mathbf{r}_{pd}|}$ is entry-wise division.

2) *Beamforming of ComA*: Assume that there are K_c planar far-field signals arriving at ComA. The i th signal's AoA is θ_i . Similar to SenA, the steering vector of ComA is

$$\bar{\mathbf{a}}(\theta_i) = \left[1, e^{j\frac{2\pi}{\lambda}d_c \cos \theta_i}, \dots, e^{j\frac{2\pi}{\lambda}(M_{com}-1)d_c \cos \theta_i} \right]^T, \quad (7)$$

where d_c is the distance between the adjacent antennas of ComA. Then we obtain the steering matrix of ComA as $\bar{\mathbf{A}} = [\bar{\mathbf{a}}(\theta_1), \dots, \bar{\mathbf{a}}(\theta_{K_c})]$. Furthermore, the received signal of ComA can be expressed as $\mathbf{y}_c = \bar{\mathbf{A}}\mathbf{s}_c + \mathbf{n}_c$, where \mathbf{s}_c is the source signal vector of dimension $K_c \times 1$, and \mathbf{n}_c is AWGN with covariance matrix $\sigma_c^2 \mathbf{I}_{K_c}$ and zero mean. The objective for the ComA beamforming is given by

$$\min_{\mathbf{w}_c} \left\| \mathbf{w}_c^H \bar{\mathbf{A}} - \bar{\mathbf{r}}_{pd}^T \times \text{diag}(\bar{\mathbf{r}}_{ad}) \right\|_2^2, \quad (8)$$

where $\bar{\mathbf{r}}_{ad}$ and $\bar{\mathbf{r}}_{pd}$ are the desired amplitude response and desired phase response of ComB, respectively. Note that $\bar{\mathbf{r}}_{ad}$ is a column vector of real values, and $\bar{\mathbf{r}}_{pd}$ is a column vector of complex values with unit modulus. **Algorithm 1** is also applied to generate ComB. After τ_{th} iterations or \mathbf{w}_c converges to a stable value, the desired beamforming vector for ComB will be output.

D. Signal Model of the JSC CSUN

OFDM signal is adopted in the JSC CSUN to exploit its advantage of the frequency diversity and obtain high processing gain [16]. The baseband OFDM JSC signal is modeled as [16]

$$x(t) = \sum_{m=0}^{M_s-1} \sum_{q=0}^{N_c-1} d_{Tx}(mN_c+q) \exp(j2\pi f_q t) \text{rect}\left(\frac{t-mT}{T}\right), \quad (9)$$

where M_s is the number of OFDM symbols in one frame, N_c is the number of subcarriers, $d_{Tx}(mN_c+q)$ is the transmit symbol on the q th subcarrier of the m th OFDM block, B is the bandwidth of the JSC signal, $f_q = \frac{qB}{N_c}$ is the baseband frequency of the q th subcarrier, and T is the duration time of each OFDM symbol that contains guard interval and the duration of OFDM block.

The phase difference between the transmitted and the received OFDM symbols is used to estimate the Doppler frequency shift and the time delay between the target and the UAV.

The Doppler shift results from the radial relative velocity between the UAV and the target, and can be presented as

$$f_{d,s} = \frac{2v_{rel}f_c}{c_0}, \quad (10)$$

where c_0 is the speed of light, f_c is the carrier frequency of the OFDM signal, and v_{rel} is the radial relative velocity between UAV and the target. The time delay is expressed as

$$\tau_s = \frac{2R_r}{c_0}, \quad (11)$$

where R_r is the distance between the target and the UAV. The complex ratio of the received to the transmitted OFDM signal is expressed as [16]

$$(\mathbf{D}_{div})_{m,q} = \frac{d_{Rx}(mN_c+q)}{d_{Tx}(mN_c+q)}$$

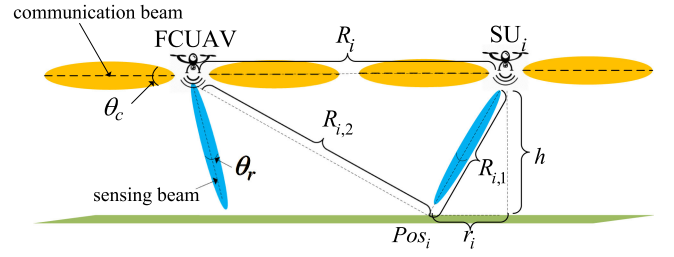


Fig. 5. Front view of vertical pattern of sensing beam and communication beam.

$$= (\mathbf{H})_{m,q} \exp(-j2\pi f_q \tau_s) \exp(j2\pi m T f_{d,s}), \quad (12)$$

where $(\cdot)_{m,q}$ is the entry of a matrix at the m th row and the q th column, $d_{Rx}(mN_c+q)$ is the received OFDM symbol corresponding to $d_{Tx}(mN_c+q)$, and $(\mathbf{H})_{m,q}$ is the complex fading factor for the q th subcarrier of the m th OFDM symbol. The matrix form of (12) is given by

$$(\mathbf{D}_{div})_{m,q} = (\mathbf{H})_{m,q} (\mathbf{k}_D \mathbf{k}_R^T)_{m,q}, \quad (13)$$

where $m = 0, 1, \dots, M_s - 1$, $q = 0, 1, \dots, N_c - 1$, $\mathbf{k}_R(q) = \exp(-j2\pi f_q \tau_s)$, and $\mathbf{k}_D(m) = \exp(j2\pi m T f_{d,s})$.

By applying discrete Fourier transform (DFT) to each column of \mathbf{D}_{div} and inverse discrete Fourier transform (IDFT) to each row of \mathbf{D}_{div} , $f_{d,s}$ and R_r can be obtained respectively.

Let $\mathbf{D}_{m,IDFT}$ denote the IDFT of the m th row of \mathbf{D}_{div} , and $\mathbf{D}_{q,DFT}$ denote the DFT of the q th column of \mathbf{D}_{div} . The index corresponding to the peak of $\mathbf{D}_{m,IDFT}$ depends on $f_{d,s}$ and can be obtained by one-dimensional exhaustive search as follows [2]:

$$\text{ind}_{d,m} = \lfloor f_{d,s} T M_s \rfloor, \text{ind}_{d,m} = 0, 1, \dots, N_c - 1. \quad (14)$$

Similarly, the index corresponding to the peak of $\mathbf{D}_{q,DFT}$ depends on R_r and can be obtained by one-dimensional exhaustive search as follows [2]:

$$\text{ind}_{R,q} = \lfloor \frac{2R_r B}{c_0} \rfloor, \text{ind}_{R,q} = 0, 1, \dots, M_s - 1. \quad (15)$$

Based on (14) and (15), we can obtain $f_{d,s}$ and R_r , respectively. The accuracy of the estimation depends on the duration time of each OFDM symbol and the bandwidth of signal [2]. This radar echo processing technique can generate a processing gain as [2]

$$G_p = N_c M_s. \quad (16)$$

E. Modeling of Mutual Sensing Interference

In order to model the mutual sensing interference, the power spectrum of the JSC OFDM signal needs to be considered first. According to [2], the aggregate OFDM power spectrum is noise-like. For reasonable simplification, we assume that the transmitting power of the OFDM sensing signal concentrates in the baseband spectrum $[0, B]$. UAVs receive the sensing interference power imposed by all other UAVs' scattered sensing signals.

FCUAV is chosen as the reference to analyze the average sensing interference imposed on a UAV from other UAVs. As illustrated in Fig. 5, denote R_i as the distance between SU_i

and FCUAV,³ Pos_i as the intersection point between the SenB direction of SU_i and SZ of SU_i , $R_{i,1}$ as the distance between SU_i and Pos_i , $R_{i,2}$ as the distance between Pos_i and FCUAV, and r_i as the distance between Pos_i and the projection point of SU_i on SZ. We assume that the interfering sensing signals are random due to the random scattering. The sensing interfering power imposed by SU_i on FCUAV is formulated as [17], [18]

$$I_{sen,i} = \frac{P_r g_{ts}}{4\pi} R_{i,1}^{-2} \bar{\sigma} \frac{1}{4\pi} R_{i,2}^{-2} \frac{\lambda^2 g_{rs}}{4\pi}, \quad (17)$$

where g_{ts} and g_{rs} are the gains of transmitting and receiving sensing beams, respectively, $\bar{\sigma}$ is the mean of radar cross section of target, λ is the wavelength of the carrier of JSC transceiver, and $R_{i,1}$ and $R_{i,2}$ are expressed as follows:

$$R_{i,1} = \sqrt{r_i^2 + h_i^2},$$

$$R_{i,2} = \sqrt{(R_i - r_i)^2 + h^2}. \quad (18)$$

Here, $r_i, h_i, h, R_i, R_{i,1}, R_{i,2} > 0$, based on the arithmetic and geometric means (AM-GM) inequality, we have

$$I_{sen,i} \leq \frac{P_r g_{ts} g_{rs} \lambda^2 \bar{\sigma}}{(4\pi)^3} \frac{R_{i,2}^{-4} + R_{i,1}^{-4}}{2}, \quad (19)$$

where if and only if $R_{i,1}^{-2} = R_{i,2}^{-2}$, i.e., $r_i = \frac{R_i}{2} + \frac{h^2 - h_i^2}{2R_i}$, the equality holds. By combining (18) and (19), we have

$$I_{sen,i} \leq \frac{P_r g_{ts} g_{rs} \lambda^2 \bar{\sigma}}{(4\pi)^3} \left(\frac{R_i^2}{4} + \frac{(h^2 - h_i^2)^2}{4R_i^2} + \frac{h^2 + h_i^2}{2} \right)^{-2}$$

$$\leq \frac{P_r g_{ts} g_{rs} \lambda^2 \bar{\sigma}}{(4\pi)^3} \left(\frac{R_i^2}{4} + \frac{h^2 + h_i^2}{2} \right)^{-2}$$

$$= \frac{P_r g_{ts} g_{rs} \lambda^2 \bar{\sigma}}{4\pi^3} (R_i^2 + 2h^2 + 2h_i^2)^{-2}. \quad (20)$$

Moreover, the expectation of sensing interference imposed on FCUAV from M SUs can be upper bounded by

$$I_{sen} = E_{R_i} \left(\sum_{i=1}^M I_{sen,i} \right)$$

$$\leq E_{R_i} \left(\sum_{i=1}^M \frac{P_r g_{ts} g_{rs} \lambda^2 \bar{\sigma}}{4\pi^3} (R_i^2 + 2h^2 + 2h_i^2)^{-2} \right). \quad (21)$$

As the second-order derivative of $(R_i^2 + 2h^2 + 2h_i^2)^{-2}$ with regard to R_i is $24R_i^2(R_i^2 + 2h^2 + 2h_i^2)^{-4} \geq 0$ for $R_i, h_i, h > 0$, I_{sen} is convex of R_i for $R_i > 0$. By using the Jensen's inequality, we have

$$I_{sen} \leq \frac{P_r \lambda^2 \bar{\sigma} g_{ts} g_{rs}}{4\pi^3} \sum_{i=1}^M E \{ (R_i^2 + 2h^2 + 2h_i^2)^{-2} \}, \quad (22)$$

where

$$E \{ (R_i^2 + 2h^2 + 2h_i^2)^{-2} \} = \frac{(R_g^2 + 2h^2 + 2h_i^2)^{-1} - (x_{Q^2}^2 + 2h^2 + 2h_i^2)^{-1}}{x_{Q^2}^2 - R_g^2}. \quad (23)$$

The proof of (23) is provided in Theorem 1 in Appendix. The maximum mutual sensing interference can be obtained by

combining (22) and (23), as given by

$$I_{sen}^{max} = \frac{P_r \lambda^2 \bar{\sigma} g_{ts} g_{rs}}{4\pi^3} \sum_{i=1}^M [(R_g^2 + 2h^2 + 2h_i^2)(x_Q^2 + 2h^2 + 2h_i^2)]^{-1}. \quad (24)$$

From (24), we can see that the maximum mutual sensing interference decreases with the increase of the hovering altitude.

III. COOPERATIVE SENSING PERFORMANCE ANALYSIS OF THE JSC CSUN

A. Minimum Required SINR for Effective Sensing

As stated before, the power spectrum of OFDM signal is noise-like. Thus, the interference-and-noise imposed on sensing receiver of each UAV follows the Gaussian distribution, i.e., $A_{in} \sim N(0, N_s + I_{sen})$,⁴ where N_s is the thermal noise power.

The useful sensing signal power is

$$S = G_p \gamma_s (N_s + I_{sen}), \quad (25)$$

where γ_s denotes SINR of sensing, and G_p is presented in (16). We can obtain the following detection problem:

$$H_1 : y = \sqrt{S} + A_{in}$$

$$H_0 : y = A_{in}, \quad (26)$$

where hypothesis H_1 is that there is a target in the direction of sensing beam, hypothesis H_0 is the opposite, and y is the output signal of radar after processing M_s OFDM symbols. The decision rule of whether there is a target in the sensing direction can be expressed as [12]

$$y \underset{H_0}{\overset{H_1}{\gtrless}} \eta', \quad (27)$$

where η' is the decision threshold. When $y > \eta'$, the sensor accepts the hypothesis H_1 ; otherwise, the sensor accepts the hypothesis H_0 .

The false alarm rate and the detection probability are the metrics that have to be considered for detection [12], and are presented by

$$P_F = \int_{\eta'}^{\infty} f(y|H_0) dy = Q \left(\frac{\eta'}{\sqrt{N_s + I_{sen}}} \right) \quad (28)$$

and

$$P_D = \int_{\eta'}^{\infty} f(y|H_1) dy = Q \left(\frac{\eta' - \sqrt{S}}{\sqrt{N_s + I_{sen}}} \right), \quad (29)$$

respectively, where $Q(\cdot)$ is the monotonically decreasing Q-function [12]. According to (28), we have

$$\eta' = Q^{-1}(P_F) \sqrt{N_s + I_{sen}}, \quad (30)$$

where $Q^{-1}(\cdot)$ is the inverse function of Q-fucntion. By substituting (25) and (30) into (29), we can obtain P_D as

$$P_D = Q \left[Q^{-1}(P_F) - \sqrt{G_p \gamma_s} \right]. \quad (31)$$

For effective detection, P_F and P_D must be constrained as [12]

$$\begin{cases} P_F \leq \alpha_f \\ P_D \geq \alpha_D \end{cases}, \quad (32)$$

³ R_i is an independently and identically distributed (i.i.d.) variable.

⁴ $N(\mu, \sigma^2)$ is the Gaussian distribution with μ as mean and σ^2 as variance.

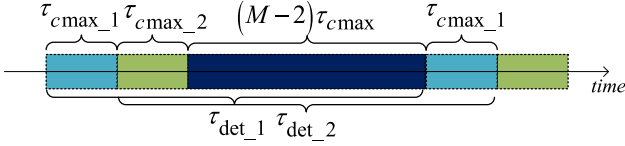


Fig. 6. Time allocation for sensing and communication.

where α_f is the maximum false alarm rate, and α_D is the minimum detection probability. Based on (31) and (32), the minimum SINR to meet the constraints can be expressed as

$$(\text{SINR})_{\min} = \frac{[Q^{-1}(\alpha_f) - Q^{-1}(\alpha_D)]^2}{G_p}. \quad (33)$$

B. Maximum Sensing Range

According to [13], the maximum sensing range of UAV is

$$R_{\max} = \left(\frac{\beta_R P g_{ts} g_{rs} (c_0/f)^2 \bar{\sigma} N_p}{(4\pi)^3 (\text{SINR})_{\min} (kT_0 F_n B + I_{\text{sen}}^{\max}) L_s} \right)^{\frac{1}{4}}, \quad (34)$$

where β_R is SPR, P is the total available radio power, g_{ts} and g_{rs} are the transmitting and the receiving antenna gains of SenB respectively, f is the carrier frequency of transceiver, $\bar{\sigma}$ is the mean radar cross section, L_s is the aggregated power loss at the propagation medium, N_p is the number of times of repeated detection, I_{sen}^{\max} is given in (24), k is the Boltzmann's constant, F_n is the noise figure of the receiver, B is the bandwidth of JSC transceiver, and $T_0 = 290$ K (in absolute temperature) is the standard temperature.

C. Maximum Cooperative Range

The time that SU requires to transmit the sensing data to FCUAV is defined as the ratio of the amount of sensing data to the communication throughput, which is

$$\tau_c(R_i) = \frac{V_{\text{data}} \tau_{\text{det}}}{T_c(R_i)}, \quad (35)$$

where V_{data} is the generating rate of the sensing data, τ_{det} is the detection time, and $T_c(R_i)$ is the throughput of the communication link between FCUAV and SU_i . As R_i increases, $T_c(R_i)$ decreases because the received ComB power decreases.

We adopt TDMA for SUs to transmit the sensing data to FCUAV. Each SU must transmit the sensing data in the assigned time slots of length $\tau_{c\max}$. SUs carry out downward-looking detection continuously as they transmit the sensing data.

Fig. 6 illustrates the time slots allocated to SUs for transmitting sensing data to FCUAV. Let $\tau_{\text{det},i}$ and $\tau_{c\max,i}$ denote the sensing slots and communication slots for SU_i , respectively. All UAVs are provided with the same sensing time τ_{det} and transmission time $\tau_{c\max}$. In order to ensure the consecutive detection of each UAV, there is

$$\tau_{c\max} = \frac{1}{M} \tau_{\text{det}}. \quad (36)$$

In this case, after SU_i completes the sensing tasks in $\tau_{\text{det},i}$, the next slot for SU_i to transmit sensing data comes again.

Based on (35), (36) and $\tau_c \leq \tau_{c\max}$, we obtain $T_c(R_i) \geq M \times V_{\text{data}}$. Thus, the distance between FCUAV

and each SU is no larger than MCR, i.e.,

$$x_Q = T_c^{-1}(M \times V_{\text{data}}), \quad (37)$$

where $T_c^{-1}(\cdot)$ is the inverse function of $T_c(R_i)$ and will be presented in the next subsection.

D. Derivation of MCR

In this subsection, we obtain the ultimate expression of MCR with respect to SU number and SPR based on the outage capacity of the CSUN. The power of communication signal received by FCUAV is

$$P_0 = P_c g_c h_c x_0^{-\alpha}, \quad (38)$$

where P_c is the power of ComB, α is the path loss exponent, g_c is the directional gain of the communication link, h_c is the small scale fading factor that follows Rician distribution with Rician factor K_h , and x_0 is the distance between the transmitter and FCUAV. We have $g_c = g_{tc} \times g_{rc}$, where g_{tc} and g_{rc} are the directional gains of transmitting ComB and receiving ComB, respectively. The PDF of h_c is expressed as follows [19]:

$$f_{h_c}(w) = \frac{(K_h + 1) e^{-K_h}}{\Omega} e^{-\frac{(K_h + 1)w}{\Omega}} I_0 \left(2\sqrt{\frac{K_h(K_h + 1)w}{\Omega}} \right), \quad (39)$$

where $I_0(x) = \sum_{n=0}^{\infty} \frac{(x/2)^{2n}}{n! \Gamma(n+1)}$ is the 0-th order modified Bessel function of the first kind, $K_h = v^2 / \sigma_K^2$, $\bar{\Omega} = 2\sigma_K^2 + v^2$ is the normalized power, v^2 denotes the strong line-of-sight (LOS) power, and σ_K^2 represents the multipath reflected power [20]–[22].

The successful transmission probability (STP) is defined as the probability that the received SNR (or SINR) is larger than a threshold γ that is necessary for successful transmission [19], [23], i.e.,

$$\begin{aligned} \rho_c^s(x_0, \gamma) &= \Pr \left(\frac{P_0}{N_{\text{com}}} > \gamma \right) \\ &= \Pr \left(h_c > \frac{\gamma N_{\text{com}}}{P_c g_c} x_0^\alpha \right), \end{aligned} \quad (40)$$

where N_{com} is the noise power at communication receiver. Since h_c follows Rician distribution with Rician factor K_h , STP is formulated as [20]

$$\rho_c^s(x_0, \gamma) = Q \left(\sqrt{2K_h}, \sqrt{\frac{2\gamma(1 + K_h)x_0^\alpha N_{\text{com}}}{g_c P_c}} \right), \quad (41)$$

where $Q(a_1, a_2)$ is the first order Marcum Q-function. The outage probability is the complement of ρ_c^s , i.e.,

$$\rho_c^{\text{out}} = 1 - \rho_c^s(x_0, \gamma). \quad (42)$$

The outage capacity is written as [23]

$$T_C(x_0) = B(1 - \varepsilon) \log_2(1 + \gamma_{th}), \quad (43)$$

where B is the available bandwidth of the JSC transceiver, ε is the maximum of ρ_c^{out} , and γ_{th} is the SNR threshold that makes the outage probability equal to ε [23]. If $\gamma > \gamma_{th}$, then the outage probability will be larger than ε . Combining (41), (42) and (43),

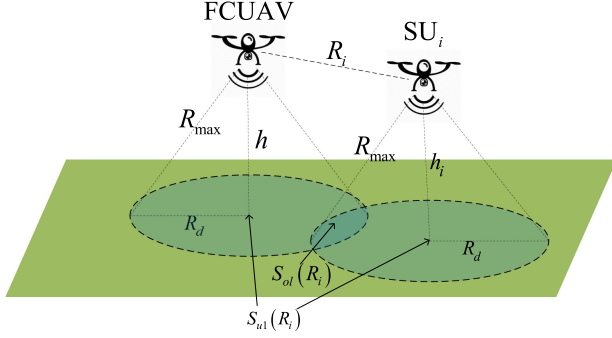


Fig. 7. Illustration of cooperative sensing of the S-C pair.

we have

$$T_c(x_0) = B(1 - \varepsilon) \log_2 \left(1 + \frac{g_c P_c [Q^{-1}(\sqrt{2K_h}, 1 - \varepsilon)]^2}{2(1 + K_h) x_0^\alpha N_{com}} \right), \quad (44)$$

where $Q^{-1}(\cdot, \cdot)$ is the inverse function of $Q(a_1, a_2)$ with regard to a_2 ,⁵ and $T_c(x_0)$ is the communication performance metric of the JSC CSUN.

Based on (37) and (44), we obtain MCR, x_Q , which is equal to the specific value of x_0 that satisfies $T_c(x_0) = M \times V_{data}$. We can obtain x_Q as

$$x_Q = \left[\frac{g_c(1 - \beta_R)P[Q^{-1}(\sqrt{2K_h}, 1 - \varepsilon)]^2}{2(1 + K_h)N_{com} \left(2^{\frac{MV_{data}}{B(1 - \varepsilon)}} - 1 \right)} \right]^{1/\alpha}. \quad (45)$$

E. Cooperative Sensing Performance Analysis

We denote an SU and FCUAV that communicates sensing data as an S-C pair. As shown in Fig. 7, the SZ radius of the i th SU is formulated as

$$R_{d,i}(h_i) = \sqrt{(R_{\max})^2 - h_i^2} \times [u(R_{\max} - h_i)], \quad (46)$$

where $u(\cdot)$ is the step function,⁶ and R_{\max} is given in (34). For analytical tractability, we assume $h_i = h$, thus all SUs have the same SZ radius as FCUAV, i.e.,

$$R_d = R_{d,i}(h). \quad (47)$$

Subsequently, the overlapped area between SZs of the S-C pair can be expressed as

$$S_{ol}(R_i) = \left[2R_d^2 \arccos\left(\frac{R_i}{2R_d}\right) - R_i \sqrt{R_d^2 - \left(\frac{R_i}{2}\right)^2} \right] \times u(2R_d - R_i). \quad (48)$$

Then, the union area of SZs of the S-C pair is

$$S_{u1}(R_i) = 2\pi R_d^2 - S_{ol}(R_i). \quad (49)$$

The expectation of $S_{u1}(R_i)$, for $R_g \leq R_i < x_Q$, is defined as the sensing performance metric of the S-C pair, which is

⁵As $Q(a_1 a_2)$ is a monotonically decreasing function of a_2 [24], the inverse function of the first order Marcum Q-function with regard to a_2 exists. If $b_1 = Q^{-1}(\sqrt{2K_h}, 1 - \varepsilon)$, then $Q(\sqrt{2K_h}, b_1) = 1 - \varepsilon$.

⁶i.e., when there is $x \geq 0$, $u(x) = 1$; otherwise, $u(x) = 0$.

formulated as [1]

$$E_S(x_Q) = \int_{R_g}^{x_Q} f_{R_i}(r) S_{u1}(r) dr = \begin{cases} F_1(x_Q), & x_Q < 2R_d \\ F_2(x_Q), & x_Q \geq 2R_d \end{cases}, \quad (50)$$

where $f_{R_i}(r) = \frac{2r}{x_Q^2 - R_g^2}$ for $R_g < r < x_Q$, is the probability density function (PDF) of R_i . Moreover, $F_1(x_Q)$ and $F_2(x_Q)$ are given in (51) and (52), shown at the bottom of the next page, respectively.

There are M S-C pairs located in MCA. The average cooperative sensing area of the JSC CSUN is defined as the average union area of SZs of M S-C pairs. Because it is extremely intractable to obtain an explicit expression for the average union area of a certain number of randomly distributed circle areas. For tractability, we merely subtract the overlapped sensing area between each SU and FCUAV to obtain the UB-ACSA as the sensing performance metric of the JSC CSUN. UB-ACSA is obtained as [1]

$$\begin{aligned} \overline{S_u}(M) &= E_{\mathbf{R}} \left\{ \sum_{i=1}^M [S_{u1}(R_i) - S(R_d)] \right\} + S(R_d) \\ &= M \times E_S(x_Q) - (M - 1)S(R_d), \end{aligned} \quad (53)$$

where $S(R_d) = \pi R_d^2$ is the area of SZ of each UAV, and $\mathbf{R} = (R_1, R_2, \dots, R_M)$ is the multiple random variables composed of the distances between SUs and FCUAV. Each element of \mathbf{R} is an i.i.d. variable.

Based on (46), (47), and (50), the closed-form expression for UB-ACSA can be derived. UB-ACSA can be achieved when all SUs do not have overlapped SZs, which requires FCUAV to coordinate the trajectory of each SU. The JSC CSUN can detect the zone with area of UB-ACSA in much shorter time than individual UAV.

IV. NUMERICAL RESULTS

In this section, numerical and Monte-Carlo simulations are conducted to verify the theoretical analysis in the previous sections and to show the impact of the number of SUs M , the SPR β_R and the flying altitude h on UB-ACSA. The parameters used in the simulations are listed in Table II [13], [22], [25]. According to (33), the minimum required SINR for sensing, i.e., SINR_{\min} , is 0.1230.

Fig. 8 shows the 3D beam pattern of SenB. The azimuth and elevation beamwidths of SenB are approximately 4.5 and 5 degrees, respectively. Based on the beam pattern of SenB, we can obtain the average gain of the mainlobe of SenB as approximately 127.4 (in decimal), i.e., $g_{ts} = g_{rs} = 127.4$.

Fig. 9 shows the 2D beam pattern of ComB. The elevation beamwidth of ComB is approximately 9 degrees. The average gain of the mainlobe of ComB is approximately 8.5, i.e., $g_c = 8.5$.

Fig. 10 plots both the theoretical and simulation results of UB-ACSA changing versus β_R , when $K_h = 10$ and $h = 150$ m, under different given M . Each curve can be generally divided

TABLE II
SIMULATION PARAMETERS

Parameter Items	Value	Description
P	10 W	The total available power
N_{com}	- 94 dBW	The power of AWGN for communication
γ	2	The threshold for STP
M_s	16	The number of OFDM symbols in a frame
N_c	64	The number of subcarriers
G_p	1024	The processing gain of sensing
M_{com}	16	The number of antennas of ComA
N_A	17	The number of layers of SenA
2^b	16	The number of antennas of the SenA layer
α_f	10^{-8}	The maximum false alarm rate
α_D	0.99999999	The minimum detection probability
α	2.6	The path loss exponent
ε	0.1	The maximum outage probability
f_c	24 GHz	The carrier frequency
$\bar{\sigma}$	1	The average RCS
F_n	10	The noise figure of receiver
T_0	290 K	The standard temperature
B	200 MHz	The bandwidth of transceiver
V_{data}	1 M Byte/s	The generating rate of sensing data
K_h	10 dB	The Rician factor
L_s	1	The propagation loss
N_p	1	The number of times of repeated detection

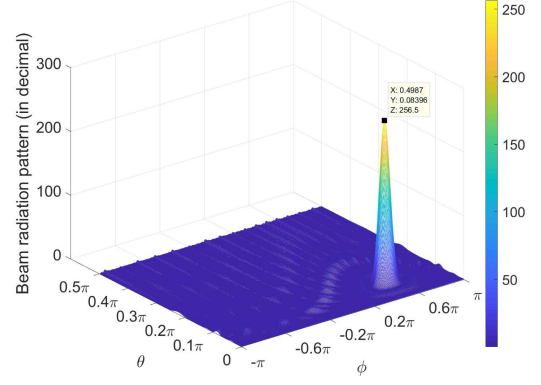


Fig. 8. 3D beam radiation pattern of SenB over AoAs in radians.

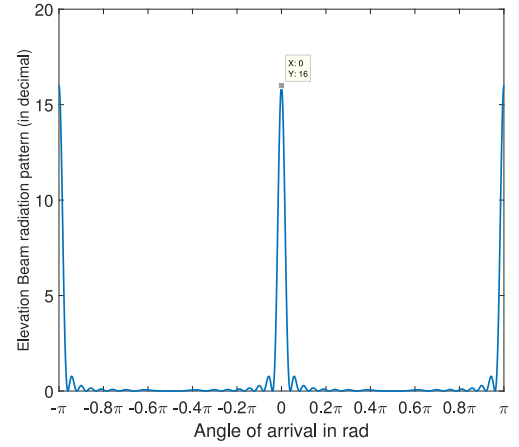


Fig. 9. Beam pattern of ComB over AoAs in radians.

into three stages given M . In the first stage where β_R is low, the power of ComB is large. Then x_Q is large enough for UAVs to expand the sensing zone. Thus, UB-ACSA increases with the increase of β_R . In the second stage where β_R is too large, UB-ACSA decreases as β_R increases, because the mutual sensing interference, I_{sen} , increases and R_{max} decreases as

the SenB power increases and x_Q decreases. When β_R is so large that $R_{max} < h$ holds, the third stage appears. UB-ACSA decreases and converges to 0 m², because I_{sen} is extremely large. Obviously, it is better to only deploy a FCUAV to sense the environment with no mutual sensing interference. In Fig. 10, the maximum point of each curve is marked in red diamond. When

$$\begin{aligned}
 F_1(x_Q) = & \frac{1}{4(x_Q^2 - R_g^2)} \left\{ x_Q \sqrt{4R_d^2 - x_Q^2} (2R_d^2 + x_Q^2) + 8\pi R_d^2 x_Q^2 + 8R_d^2 \left[R_g^2 \arccos\left(\frac{R_g}{2R_d}\right) - x_Q^2 \arccos\left(\frac{x_Q}{2R_d}\right) \right] \right. \\
 & + 8R_d^4 \left[2\arcsin\left(\frac{R_g}{2R_d}\right) + \operatorname{arccot}\left(\frac{\sqrt{4R_d^2 - x_Q^2}}{x_Q}\right) - \operatorname{arccot}\left(\frac{\sqrt{4R_d^2 - R_g^2}}{R_g}\right) - 2\arcsin\left(\frac{x_Q}{2R_d}\right) \right] \\
 & \left. - R_g \sqrt{4R_d^2 - R_g^2} (2R_d^2 + R_g^2) - 8\pi R_d^2 R_g^2 \right\}
 \end{aligned} \tag{51}$$

$$\begin{aligned}
 F_2(x_Q) = & \frac{1}{x_Q^2 - R_g^2} \left\{ 2\pi R_d^2 (x_Q^2 - R_g^2) + \pi R_d^4 - 2R_d^4 \operatorname{arccot}\left(\frac{\sqrt{4R_d^2 - R_g^2}}{R_g}\right) \right. \\
 & \left. - 2R_d^2 \arccos\left(\frac{R_g}{2R_d}\right) (2R_d^2 - R_g^2) - \frac{1}{4} R_g \sqrt{4R_d^2 - R_g^2} [2R_d^2 + R_g^2] \right\}
 \end{aligned} \tag{52}$$

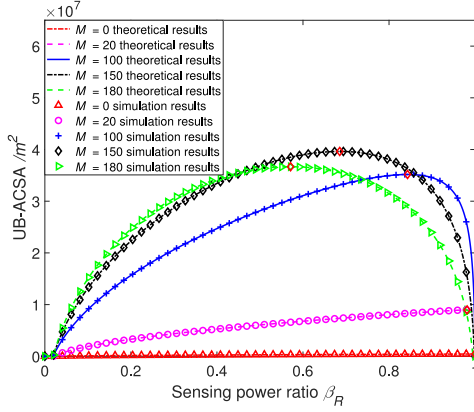


Fig. 10. UB-ACSA changes with SPR β_R under different SU number M when $K_h = 10$ and $h = 150$ m.

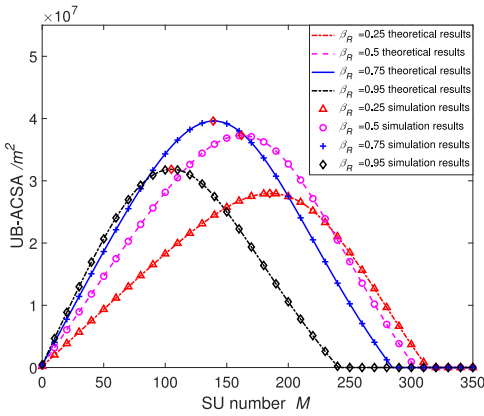


Fig. 11. UB-ACSA changes with SU number M under different SPR β_R when $K_h = 10$ and $h = 150$ m.

the JSC CSUN contains 150 SUs, the maximum UB-ACSA is 3.963×10^7 m², which is achieved when there is $\beta_R = 0.6854$.

Fig. 11 demonstrates both the analytical and simulation results of UB-ACSA changing versus M under different β_R , when $K_h = 10$ and $h = 150$ m. Each curve of UB-ACSA has three stages. In the first stage where M is relatively small, UB-ACSA increases fast and linearly as M increases. This results from that x_Q is considerably large, because there are fewer SUs requiring to transmit the sensing data. When M gets too large, the second stage comes, where x_Q is much smaller. UB-ACSA decreases fast as M increases, because I_{sen} gets larger. If M is so large that I_{sen} becomes extremely large, then R_d converges to 0 m. Therefore, UB-ACSA will become 0 m² hereafter, which is the third stage. Fewer SUs are needed to reach the maximum UB-ACSA as β_R increases, because if the ComB power decreases, then fewer SUs can be supported to transmit sensing data to FCUAV. As β_R increases, it takes fewer SUs to make R_d be 0 m, because the larger SenB power and smaller x_Q lead to the increase of I_{sen} . In Fig. 11, the maximum point of each curve is marked in red diamond. When β_R is 0.75, the optimal value of M is 139, which makes UB-ACSA reach the maximum value, 3.959×10^7 m².

Fig. 12 shows the results of UB-ACSA changing with the hovering altitude h under different M when $\beta_R = 0.5$, $h \in$

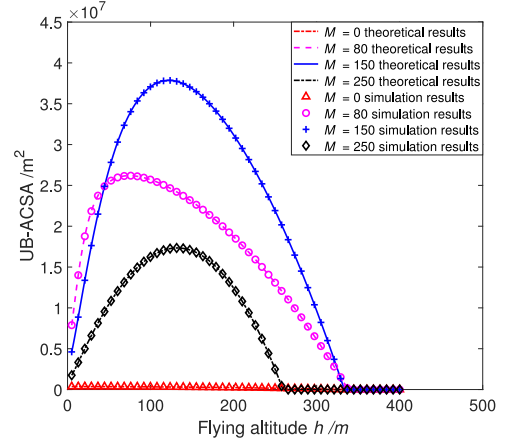


Fig. 12. UB-ACSA changes with hovering altitude h under different SU number M when $K_h = 10$ and $\beta_R = 0.5$.

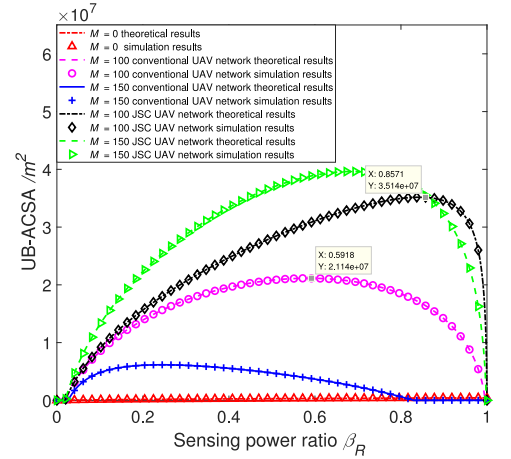


Fig. 13. UB-ACSA results of our proposed JSC CSUN and the conventional CSUN changing with SPR β_R under different SU number M when $K_h = 10$ and $h = 150$ m.

[5400]m [22]. As h increases, UB-ACSA first increases to the maximum and then gradually decreases. This is because I_{sen} decreases as h increases, and R_{max} increases faster at a lower altitude. However, when h is high, I_{sen} approaches 0 and the increase rate of R_{max} becomes slower, UB-ACSA is thus flattened, and then gradually decreases as h increases. Moreover, as M increases, we can find that the increase rate of UB-ACSA at low altitude becomes slower. This results from that as M increases, I_{sen} increases.

Fig. 13 shows the comparison between the UB-ACSA of the conventional CSUN and our proposed JSC CSUN. It is seen that a single UAV cannot achieve cooperative sensing. Thus, the sensing area of a single UAV is UB-ACSA of a FCUAV, i.e., $M = 0$ in Fig. 13. The conventional CSUN is assumed to be equipped with individually designed radar sensing and communication modules, i.e., radar sensing and communication use separate spectrum and transceivers [5]. Compared with the conventional CSUN, the JSC CSUN can merge the spectrum of radar and communication with beam sharing scheme, and thus has larger spectrum for communication than the conventional CSUN. Therefore, the JSC CSUN can provide higher throughput

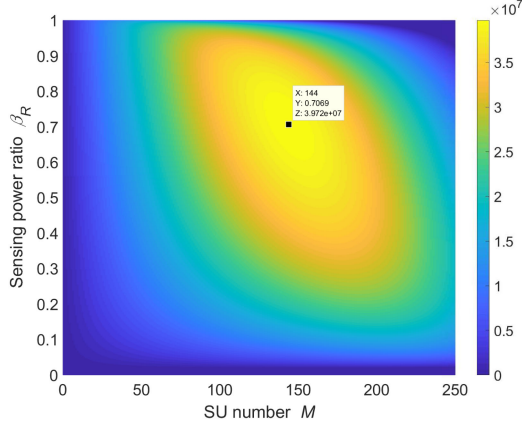


Fig. 14. UB-ACSA changes with SPR β_R and SU number M when $K_h = 10$ and $h = 150$ m.

and has larger cooperative sensing range x_Q and UB-ACSA than the conventional CSUN under the same number of SUs.

Fig. 14 presents the results of UB-ACSA changing versus β_R and M . On the one hand, when β_R and M are relatively small, the communication capacity is much larger than the requirement for sensing data integration. Thus, the communication capacity for data integration is not completely exploited, i.e., UB-ACSA cannot reach the maximum when β_R and M are small. On the other hand, too large β_R will result in the decrease of UB-ACSA because x_Q is too small. When M is too large, x_Q also becomes quite small, and I_{sen} thus becomes large enough to make R_{max} decreases to a small value. As a result, when M and β_R are too large, UB-ACSA will decrease enormously as M and β_R increase. In Fig. 14, when $\beta_R = 0.7069$ and $M = 144$, UB-ACSA reaches the maximum value of 3.972×10^7 m². In the above procedure, we can easily determine the optimal values of β_R and M to achieve the optimal UB-ACSA.

V. CONCLUSION

This work has put forward a JSC CSUN based on beam sharing scheme to enhance the cooperative sensing performance of CSUN. To achieve beam sharing JSC scheme, we have proposed a novel design of JSC antenna array that consists of the communication subarray and sensing subarray and put forward corresponding beamforming algorithm. To quantify the cooperative sensing performance of CSUN, we have proposed and derived a novel UB-ACSA as the cooperative sensing performance metric of CSUN. Through simulation, we have validated our theoretical results of UB-ACSA, and shown that UB-ACSA increases first and then decreases with the increase of SU number, hovering altitude and SPR. The optimal values of these three parameters can be identified numerically. Moreover, we have presented that the UB-ACSA of the JSC CSUN improves 66.3 percent compared to the conventional CSUN.

APPENDIX A

Theorem 1: A 2D uniform point process is generated within a concentric circle area whose inner radius and outer radius are R_g

and x_Q , respectively. The distance between a generated point and the center is denoted by R_i . Let h and h_i denote positive constant parameters. Then the expectation of $Y = (R_i^2 + 2h^2 + 2h_i^2)^{-2}$ of R_i is

$$E(Y) = \frac{(R_g^2 + 2h^2 + 2h_i^2)^{-1} (x_Q^2 + 2h^2 + 2h_i^2)^{-1}}{x_Q^2 - R_g^2}.$$

Proof: The cumulative density function of R_i should be $F_{R_i}(r) = \frac{r^2 - R_g^2}{x_Q^2 - R_g^2} (R_g < r < x_Q)$. Thus, the cumulative distribution function of $Y = (R_i^2 + 2h^2 + 2h_i^2)^{-2}$ ($h, h_i > 0$ and $R_g < R_i < x_Q$) is

$$\begin{aligned} F_Y(y) &= \Pr(Y \leq y) \\ &= \Pr(R_i^2 \geq y^{-\frac{1}{2}} - 2h^2 - 2h_i^2) \\ &= \Pr\left(R_i \geq \left(y^{-\frac{1}{2}} - 2h^2 - 2h_i^2\right)^{\frac{1}{2}}\right) \\ &= 1 - \frac{\left(y^{-\frac{1}{2}} - 2h^2 - 2h_i^2\right) - R_g^2}{x_Q^2 - R_g^2}, \end{aligned} \quad (54)$$

where $(x_Q^2 + 2h^2 + 2h_i^2)^{-2} \leq y \leq (R_g^2 + 2h^2 + 2h_i^2)^{-2}$. Then, the probability density function of Y is

$$f_Y(y) = \frac{d[F_Y(y)]}{dy} = \frac{1}{2(x_Q^2 - R_g^2)} y^{-\frac{3}{2}}, \quad (55)$$

where $(x_Q^2 + 2h^2 + 2h_i^2)^{-2} \leq y \leq (R_g^2 + 2h^2 + 2h_i^2)^{-2}$. Thus, the expectation of Y is

$$\begin{aligned} E(Y) &= \int_{(x_Q^2 + 2h^2 + 2h_i^2)^{-2}}^{(R_g^2 + 2h^2 + 2h_i^2)^{-2}} y f_Y(y) dy \\ &= \frac{1}{x_Q^2 - R_g^2} \left[(R_g^2 + 2h^2 + 2h_i^2)^{-1} (x_Q^2 + 2h^2 + 2h_i^2)^{-1} \right]. \end{aligned} \quad (56)$$

■

REFERENCES

- [1] X. Chen, Z. Wei, Z. Fang, H. Ma, Z. Feng, and H. Wu, "Performance of joint radar-communication enabled cooperative UAV network," in *Proc. IEEE Int. Conf. Signal, Inf. Data Process.* 2019, Dec. 2019, pp. 1–4.
- [2] C. Sturm and W. Wiesbeck, "Waveform design and signal processing aspects for fusion of wireless communications and radar sensing," *Proc. IEEE*, vol. 99, no. 7, pp. 1236–1259, May 2011.
- [3] L. Han and K. Wu, "Joint wireless communication and radar sensing systems state-of-the-art and future prospects," *IET Microw., Antennas Propag.*, vol. 7, no. 11, pp. 876–885, Aug. 2013.
- [4] F. Liu, C. Masouros, A. Petropulu, H. Griffiths, and L. Hanzo, "Joint radar and communication design: Applications, state-of-the-art, and the road ahead," *IEEE Trans. Commun.*, vol. 68, no. 6, pp. 3834–3862, Jun. 2020.
- [5] H. Hildmann and E. Kovacs, "Using unmanned aerial vehicles (UAVs) as mobile sensing platforms (MSPs) for disaster response, civil security and public safety," *Drones*, vol. 3, no. 3, p. 59, Jul. 2019.
- [6] C. Sturm, T. Zwick, and W. Wiesbeck, "An OFDM system concept for joint radar and communications operations," *VTG Spring*, pp. 1–5, Apr. 2009.
- [7] J. Moghaddasi and K. Wu, "Multifunctional transceiver for future radar sensing and radio communicating data-fusion platform," *IEEE Access*, vol. 4, pp. 818–838, 2016.
- [8] J. A. Zhang, X. Huang, Y. J. Guo, J. Yuan, and R. W. Heath, "Multibeam for joint communication and radar sensing using steerable analog antenna arrays," *IEEE Trans. Veh. Technol.*, vol. 68, no. 1, pp. 671–685, Jan. 2019.
- [9] F. Liu, C. Masouros, A. Li, H. Sun, and L. Hanzo, "MU-MIMO communications with MIMO radar: From co-existence to joint transmission," *IEEE Trans. Wireless Commun.*, vol. 17, no. 4, pp. 2755–2770, Feb. 2018.

- [10] F. Causa, A. R. Vetrella, G. Fasano, and D. Accardo, "Multi-UAV formation geometries for cooperative navigation in GNSS-challenging environments," *IEEE/ION Position, Location Navigation Symp.* pp. 775–785, Apr. 2018.
- [11] C. Kanellakis, S. S. Mansouri, E. Fresk, D. Kominaki, and G. Nikolakopoulos, "Cooperative UAVs as a tool for aerial inspection of large scale aging infrastructure," *IEEE/RSJ Int. Conf. Intell. Robots Syst. (IROS)*, p. 5040, Oct. 2018.
- [12] B. C. Levy, *Principles of Signal Detection and Parameter Estimation*. Boston, MA, USA: Springer Sci. Bus. Media, 2008, pp. 1–644.
- [13] M. A. Richards, J. Scheer, W. A. Holm, and W. L. Melvin, *Principles of Modern Radar: Basic Principles*. Georgia, USA: Radar, Sonar & Navigation, 2010, pp. 1–925.
- [14] Z. Zhang, X. Chai, K. Long, A. V. Vasilakos, and L. Hanzo, "Full duplex techniques for 5G networks: Self-interference cancellation, protocol design, and relay selection," *IEEE Commun. Mag.*, vol. 53, no. 5, pp. 128–137, May 2015.
- [15] Z. Shi and Z. Feng, "A new array pattern synthesis algorithm using the two-step least-squares method," *IEEE Signal Process. Lett.*, vol. 12, no. 3, pp. 250–253, Mar. 2005.
- [16] C. Sturm, T. Zwick, W. Wiesbeck, and M. Braun, "Performance verification of symbol-based OFDM radar processing," in *Proc. IEEE Radar Conf.*, May 2010, pp. 60–63.
- [17] M. A. Richards, *Fundamentals of Radar Signal Processing*. New York, NY, USA: Tata McGraw-Hill Edu., 2005, pp. 1–539.
- [18] A. F. Molisch, *Wireless Communications*. New Jersey, NJ, USA: John Wiley & Sons, 2012, pp. 1–884.
- [19] X. Yuan *et al.*, "Capacity analysis of UAV communications: Cases of random trajectories," *IEEE Trans. Veh. Technol.*, vol. 67, no. 8, pp. 7564–7576, Aug. 2018.
- [20] M. M. Azari, F. Rosas, K.-C. Chen, and S. Pollin, "Ultra reliable UAV communication using altitude and cooperation diversity," *IEEE Trans. Commun.*, vol. 66, no. 1, pp. 330–344, Jan. 2018.
- [21] N. Goddemeier and C. Wietfeld, "Investigation of air-to-air channel characteristics and a UAV specific extension to the Rice model," in *Proc. IEEE Globecom Workshops*, Dec. 2015, pp. 1–5.
- [22] A. A. Khuwaja, Y. Chen, N. Zhao, M.-S. Alouini, and P. Dobbins, "A survey of channel modeling for UAV communications," *IEEE Commun. Surv. Tut.*, vol. 20, no. 4, pp. 2804–2821, Oct.–Dec. 2018.
- [23] S. Zhalehpour, M. Uysal, O. A. Dobre, and T. Ngatched, "Outage capacity and throughput analysis of multiuser FSO systems," in *Proc. IEEE 14th Can. Workshop Inf. Theory*, Jul. 2015, pp. 143–146.
- [24] D. A. Shnidman, "The calculation of the probability of detection and the generalized marcum Q-function," *IEEE Trans. Inf. Theory*, vol. 35, no. 2, pp. 389–400, Mar. 1989.
- [25] V. Lakshmanan, "Overview of radar data compression," *Satell. Data Compression, Commun., Archiving III*, vol. 6683, pp. 1–5, Sep. 2007.

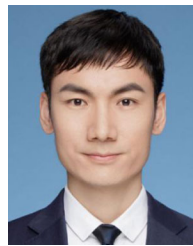


Xu Chen (Student Member, IEEE) received the B.S. degree from Southwest Jiaotong University, Chengdu, China, in 2018. He is currently working toward the Ph.D. degree from the Beijing University of Posts and Telecommunications, Beijing, China. His research interests include wireless communication, machine-type communication, sensor network, joint communication and sensing network, and signal processing.



Zhiyong Feng (Senior Member, IEEE) received the B.E., M.E., and Ph.D. degrees from the Beijing University of Posts and Telecommunications (BUPT), Beijing, China. She is currently a Professor with BUPT, and the Director of the Key Laboratory of the Universal Wireless Communications, Ministry of Education, China. She is the Vice Chair of the Information and Communication Test Committee of the Chinese Institute of Communications (CIC). She is currently an Associate Editor-in-Chief for *China Communications*, and she is a Technological Advisor

for International Forum on NGMN. Her main research interests include wireless network architecture design and radio resource management in 5th generation mobile networks, spectrum sensing and dynamic spectrum management in cognitive wireless networks, and universal signal detection and identification.



Wireless Communications and Signal Processing 2018. He was the Registration Co-Chair of the IEEE/CIC International Conference on Communications in China (ICCC) 2018, and the Publication Co-Chair of IEEE/CIC ICC 2019.

Zhiqing Wei (Member, IEEE), received the B.E. and Ph.D. degrees from the Beijing University of Posts and Telecommunications (BUPT), Beijing, China, in 2010 and 2015, respectively. He is currently an Associate Professor with BUPT. He has authored or coauthored one book, three book chapters, and more than 50 papers. His research interests include performance analysis and optimization of mobile ad hoc networks. He was granted the Exemplary Reviewer of IEEE WIRELESS COMMUNICATIONS LETTERS in 2017, the Best Paper Award of the International Conference on



Feifei Gao (Fellow, IEEE) received the B.Eng. degree from Xi'an Jiaotong University, Xi'an, China, in 2002, the M.Sc. degree from McMaster University, Hamilton, ON, Canada, in 2004, and the Ph.D. degree from the National University of Singapore, Singapore, in 2007. Since 2011, he has been an Associate Professor with the Department of Automation, Tsinghua University, Beijing, China.

His research interests include signal processing for communications, array signal processing, convex optimizations, and artificial intelligence-assisted

communications. Dr. Gao was an Editor of IEEE TRANSACTIONS ON WIRELESS COMMUNICATIONS, the Lead Guest Editor for IEEE JOURNAL OF SELECTED TOPICS IN SIGNAL PROCESSING and IEEE TRANSACTIONS ON COGNITIVE COMMUNICATIONS AND NETWORKING, and a Senior Editor of IEEE SIGNAL PROCESSING LETTERS, IEEE COMMUNICATIONS LETTERS, IEEE WIRELESS COMMUNICATIONS LETTERS, and *China Communications*. He was the Symposium Co-Chair for 2019 IEEE Conference on Communications (ICC), 2018 IEEE Vehicular Technology Conference Spring (VTC), 2015 IEEE Conference on Communications (ICC), 2014 IEEE Global Communications Conference (GLOBECOM), 2014 IEEE Vehicular Technology Conference Fall (VTC), and Technical Committee Member for more than 50 IEEE conferences.



Xin Yuan (Member, IEEE) received the B.E. degree from the Taiyuan University of Technology, Shanxi, China, in 2013, and the dual Ph.D. degrees from the Beijing University of Posts and Telecommunications, Beijing, China, and the University of Technology Sydney, Sydney, Australia, in 2019 and 2020, respectively. She is currently a Research Scientist with CSIRO, Australia. Her research interests include unmanned aerial vehicle (UAV) communication and networking, modelling, and performance analysis of UAV networks.